Structural and Fatigue Analysis of Jointed Plain Concrete Pavement Top-Down and Bottom-Up Transverse Cracking Subjected to Superloads

Yongsung Koh
Ph.D. student, Graduate Research Assistant (Corresponding Author)
Department of Civil, Construction and Environmental Engineering (CCEE)
24 Town Engineering Building
Iowa State University, Ames, IA 50011-1066
E-mail: yskho27@iastate.edu
ORCID: 0000-0003-0582-1898

Halil Ceylan, Ph.D.**,** F.ASCE
Pitt-Des Moines, Inc. Endowed Professor in CCEE
Director, Program for Sustainable Pavement Engineering and Research (PROSPER)
ISU Site Director, Partnership to Enhance General Aviation Safety, Accessibility and Sustainability (PEGASAS)
410 Town Engineering Building
Iowa State University, Ames, IA 50011-1066
E-mail: hceylan@iastate.edu
ORCID: 0000-0003-1133-0366

Sunghwan Kim, Ph.D., P.E.
Associate Director of PROSPER
24 Town Engineering Building
Institute for Transportation
Iowa State University, Ames, IA 50011-1066
E-mail: sunghwan@iastate.edu
ORCID: 0000-0002-1239-2350

In Ho Cho, Ph.D.
Associate Professor, CCEE
326 Town Engineering Building
Structural Engineering and Intelligent Infrastructure Engineering
Iowa State University, Ames, IA 50011-1066
E-mail: icho@iastate.edu
ORCID: 0000-0002-2265-9602

(Word count: Text: 7,126; Tables: 250×7 = 1,750; Total: 8,876)

Submitted [08/01/2021]

ABSTRACT
Superheavy vehicles, also called superloads, have non-standardized loading configurations as well as high gross vehicle weights (GVW) and axle loadings, all of which may cause unexpectedly greater distresses on Jointed Plain Concrete Pavements (JPCP) than those caused by conventional vehicle class types categorized by the Federal Highway Administration (FHWA). In general, superloads include "Implements of Husbandry" and "Superheavy Loads", both known to be the main types of heavy transport vehicles in the Midwestern region of the U.S. To characterize non-standardized loading configurations of superloads, a mechanistic analysis approach is needed for predicting potential damages to JPCPs. In this paper, critical loading locations are determined and categorized according to the superload loading configuration for each superload generating critical pavement responses for both bottom-up transverse cracking and top-down transverse cracking. Critical pavement responses of JPCPs under critical loading conditions for each superload are calculated by performing finite-element analysis and then converted to damage ratios by comparing them with critical pavement responses resulting from FHWA class 9 truck loading using various available transfer functions based on concrete fatigue test results. The resulting critical loading location for each superload category can then easily be derived and the potential for damaging the JPCP pavement systems by each superload can be determined by comparing fatigue damage ratios.

Keywords: Superloads, Jointed Plain Concrete Pavements, Finite Element Analysis, Critical Loading Location, Damage Ratio

INTRODUCTION

Unlike traditional vehicle types listed in the Federal Highway Administration (FHWA) vehicle classification scheme, vehicles carrying superheavy payloads in addition to their own weights such as agricultural products, livestock products, excavators, or even wind towers (referred to as superloads in this study) have significant potential for damaging pavement systems. The critical load factors of a superload that would affect the resulting pavement distresses vary not only with the number of tires and axles but also with other factors such as tire-pressure variation, types of vehicular tires, and suspension types (*1, 2*). The number of tires and axle configuration (e.g., single-axle, tandem-axle, tridem-axle, and quad-axle) along with their loadings are considered major factors in predicting pavement damage resulting from the use of heavy transportation vehicles that follows the current trend of using high-efficiency and large-scale transportation vehicles to transport heavy agricultural commodities or industrial products. Superloads can be distinguished from general vehicle types not only by their high gross vehicle weights (GVW) and axle loadings, both of which may exceed the state's permit limits, but also by their non-standardized configurations of tires and axles, including a wide range of dimensions with respect to number, spacing, and loading. Such non-standardized loading configurations are known to be a major factor often responsible for unexpected damage to pavement systems, especially in the Midwestern region of the U.S. (*3, 4, 5*).

Representative superload types shown in **Figure 1** are the Implements of Husbandry (IoH) and the Superheavy Load (SHL). An IoH is consists of a tractor and trailer, or just a tractor alone, in which the highest loading portion when carrying more than 50% of payload levels tends to be allocated mostly over the trailer's axle group, so most IoHs carrying cargo loads can be satisfactorily analyzed by mainly considering only their trailer loadings, permitting efficient analysis of pavement systems supporting IoHs with relatively low computational effort. A SHL, on the other hand, will have a number of tires and axles mounted on a non-divisible and non-generic body configuration to transport a superheavy cargo such as a huge engine block or a wind turbine. Because of the difficulty of standardizing an SHL in an FHWA classification, several studies have sought to properly define and permit the SHL to reduce the risk of causing unexpected pavement distresses (*6, 7*). These studies show that SHL permit criteria in the U.S. vary from state to state, with permit establishment from some states by GVW, axle weight, and tire weight, while other states base their permits on mechanistic pavement analysis reflecting actual pavement conditions (*6*). Both IoHs and SHLs tend to have (i) high GVW or single-axle weight, exceeding 96 kips or 24 kips respectively in the cases of grain carts or tank wagons operated on highways (*8*), (ii) total vehicle width, likely to exceed the pavement lane width due to a body configuration with wide transverse tire spacing or a large number of tires per axle, and (iii) slow-moving behavior that might contribute to relatively high damage on pavement systems.

Figure 1. Sample type of IoH (Kinze grain cart) and SHL (Goldhofer SL trailer).

SCOPE AND OBJECTIVE

The scope of this study was to characterize potential for bottom-up transverse cracking and top-down transverse cracking initiated on Jointed Plain Concrete Pavements (JPCP) by many types of recently-released commercial superloads. To accomplish this task, mechanistic analysis using a Finite Element Analysis (FEA) program, ISLAB 2005 (*9*), was performed to determine critical pavement responses with respect to different superloads applied to various JPCP structures.

The main FEA issue was how to apply well-defined loading inputs of each superload to obtain critical pavement responses for different Iowa JPCP structures varying in pavement properties (thickness of the Portland cement concrete [PCC] layer, transverse joint spacing, Load Transfer Efficiency [LTE], Coefficient of Thermal Expansion [CTE], composite modulus of subgrade reaction, and temperature gradients of a PCC slab). The influence line-analysis approach suggested by Byrum and Hansen (*10*) was adopted to determine the exact loading location where critical pavement responses occur for each superload, the so-called critical loading location, represented as a distance from a transverse joint. Each such critical loading location can be categorized in terms of superload type and loading configuration for each vehicle, leading to a better understanding of the relationship between the loading locations and corresponding pavement responses.

The critical pavement responses of JPCPs under each critical superload loading condition were then converted into damage ratios by comparing them with critical pavement responses resulting from FHWA class 9 truck loading. In this process, the transfer function primarily used was one derived from the results of experimental tests by Iowa State University (ISU) and sponsored by the Iowa Department of Transportation (DOT) to reflect the material properties of PCC layers used in Iowa when calculating the number of load repetitions to failure (*11, 12)*. The loading conditions of each superload were applied to the FEA model by varying the payload level from 0% to 100% of that to which each vehicle is capable. This variation allowed checking for different potential damage levels cased by different payloads for each type of superload.

Finally, to check the benefits of paved shoulders compared to granular shoulders under superloads, the critical loading locations of superloads were re-determined from the FEA matrices simulating different shoulder alternatives, and the corresponding critical pavement responses from JPCP structures representing different types of shoulder were compared. The main objectives of this study were:

- Characterize superloads according to loading configurations;
- Determine and categorize critical loading locations of superloads to seek a better understanding of the relationships between loading location and corresponding pavement responses;
- Use a large number of analysis matrices to calculate critical pavement responses that vary with respect to JPCP conditions, superload critical loading conditions, and shoulder conditions;
- Convert critical pavement responses to fatigue damage ratios representing bottom-up transverse cracking and top-down transverse cracking by comparing the number of load repetitions to failure from each superload with those resulting from FHWA class 9 truck loading using a transfer function based on previous ISU studies on PCC utilized in Iowa JPCPs (*11, 12*);
- Compare the fatigue damage ratios calculated using the Iowa-studies-based transfer function (*11, 12*) with those calculated using other generally-accepted transfer functions.

LOADING CONFIGURATION OF SUPERLOAD

Superloads investigated as loading inputs in this study were intended to include as many as possible of the types of IoH (18 types) and SHL (16 types) currently used in the Midwestern region of the U.S. **Table 1** and **Table 2**, respectively, list specified loading conditions for each type of IoH and SHL carrying a 100% payload level. The weight calculation of each payload considered the capability of specific types of payload handled by each superload. Although both types are included in the same superload category, IoH and SHL have somewhat different loading configurations and applications that distinguish the two

types into several different classes. For example, as shown in **Table 1** and **Table 2**, IoHs can be classified into grain carts, manure tankers, agricultural trailers, and agricultural trucks according to their purpose of use, while SHLs can be classified into modular and drop-deck types based on their loading configurations. Note that in **Table 2**, the heaviest axle group among all axle possibilities of SHL has been selected to represent axle and tire weights.

Table 1. Summary of detailed information of IoH carrying 100% payload level

Trailer type (payload)	Name of trailer	No. of axles	No. of tires in one axle	Axle weight (lbs)	Tire loading (lbs)	Axle spacing (in)	Tire spacing (in)
Grain cart (e.g., wheat)	Kinze 1051	1	2 (single tire)	78,100	39,050	-	96
	Kinze 1305 flotation	1	2 (single tire)	112,400	56,200	-	100
	Kinze 1305 row crop	1	4 (single tire)	115,470	28,868	-	30, 90, 30
	Balzer 1725	2	2 (single tire)	65,500	32,750	78	126
	Balzer 2550	3	2 (single tire)	62,500	31,250	78	126
	J&M 1151	1	2 (single tire)	82,500	41,250	-	120
Manure tanker (e.g., slurry)	GEA EL48-4D 4350	2	2 (single tire)	46,843	23,422	72	95
	GEA EL48-6D 6100	3	2 (single tire)	43,152	21,576	72	95
	GEA EL48-8D 7900	4	2 (single tire)	42,095	21,047	72	95
	Balzer 6800 magnum	2	2 (single tire)	60,700	30,350	86	122
	Balzer 9500 magnum	3	2 (single tire)	55,667	27,833	86	122
	NUHN QT Quad Tanks	4	2 (single tire)	65,400	32,700	76	114
Agricutural trailer (e.g., corn)	J&M 555 wagon	2	2 (single tire)	22,615	11,308	132	88
	J&M 755 wagon	2	2 (single tire)	30,125	15,063	137	92
Agricutural truck (e.g., water)	Terragator 2505	3	1, 2, 2 (single tire)	25,620	12,810	77, 230	96
	Terragator TG7300C	2	1, 2 (single tire)	28,000	14,000	202	90
	Terragator TG8400C	2	2 (single tire)	27,048	13,524	202	90
	Case 340B	3	2 (single tire)	32,550	16,275	82, 164	102

Table 2. Summary of detailed information of SHL carrying 100% payload level

Trailer type (payload)	Name of trailer	No. of axles	No. of tires in one axle	Axle weight (lbs)	Tire loading (lbs)	Axle spacing (in)	Tire spacing (in)
Single row modular (e.g., one carrying wind turbine)	Goldhofer THP/SL-S	8+	4 (single tire)	34,400	8,600	59	32, 44, 32
	Goldhofer THP/ET	8+	4 (single tire)	50,706	12,676	55	38, 22, 38
	Goldhofer PST/ES-E	8+	4 (single tire)	132,000	33,000	63	23, 34, 23
	Goldhofer THP/UT	8+	4 (dual tire)	55,116	6,890	59	41, 30, 41
	Goldhofer THP/SL-L	8+	4 (dual tire)	57,500	7,188	59	33, 38, 33
	Goldhofer THP/HL-L	8+	4 (dual tire)	57,500	7,188	59	37, 37, 37
	Goldhofer THP/SL	8+	4 (dual tire)	99,000	12,375	59	33, 38, 33
	Goldhofer THP/HL	8+	4 (dual tire)	99,200	12,400	59	37, 37, 37
Dual row modular	Two rows of Goldhofer THP/SL-S	8+	8 (single tire)	68,800	8,600	59	32, 44, 32, 48, 32, 44, 32
	Two rows of Goldhofer PST/ES-E	8+	8 (single tire)	264,000	33,000	63	23, 34, 23, 54, 23, 34, 23
	Two rows of Goldhofer THP/UT	8+	8 (dual tire)	110,232	6,890	59	41, 30, 41, 54, 41, 30, 41
	Two rows of Goldhofer THP/HL	8+	8 (dual tire)	198,400	12,400	59	37, 37, 37, 54, 37, 37, 37
Modular w/ outrigger	Goldhofer THP/HL + outrigger	8+	8 (dual tire)	99,200	6,200	59	12, 42, 37, 37, 37, 42, 12
Drop-deck type	Kalyn Siebert 13 Axle Trailer	13 (tridem axle groups)	2 (dual tire)	22,078	5,520	60	105
	Guy M. Turner dual lane 200 ton	19 (tandem axle groups)	4 (dual tire)	40,000	5,000	69	55, 91, 55
	Guy M. Turner 19 Axle trailer 125 ton	19 (tridem axle groups)	4 (dual tire)	22,400	2,800	61	55, 91, 55

KEY METHODOLOGIES FOR JPCP DAMAGE DETERMINATION UNDER SUPERLOADS

The two major JPCP fatigue-cracking types are bottom-up transverse cracking and top-down transverse cracking; both depend not only on variation in pavement properties but also on loading levels and loading locations.

In this section, the critical loading locations of each type of superload that could produce critical pavement responses for both JPCP distress types are identified. The corresponding critical pavement responses related to bottom-up transverse cracking and top-down transverse cracking from a large number of analysis matrices are also calculated using the FE rigid-pavement analysis program, ISLAB 2005 (*9*). JPCP models for FEA vary with respect to some critical inputs, including PCC layer thickness, transverse joint spacing, LTE, CTE, subgrade-reaction composite modulus, temperature gradients in a PCC slab, and loading conditions of each superload. Finally, the critical pavement responses calculated from all the analysis cases can be converted into damage ratios by comparing them with critical pavement responses resulting from FHWA class 9 truck loading, using a transfer function based on previous results from experimental testing at ISU for PCC utilized in Iowa JPCPs (*11, 12)*.

Determination of Critical Loading Location

To determine critical loading locations for all types of superloads on JPCP, multiple FE analyses were performed by stepping a set of axles across the PCC slab from one transverse joint to the next transverse joint. As shown in **Figure 2**, a set of axles for each superload was applied at 15-inch intervals to identify the exact critical loading location that could induce two types of critical pavement responses, i.e., the critical tensile stress at the bottom of the PCC layer and the critical tensile stress at the top of the PCC layer. To obtain the critical loading locations of each superload for various JPCP structures, rigid pavement models representing different transverse joint lengths (15 ft, 17 ft, and 20 ft), transverse joint LTE (50% LTE representing transverse joint without dowel bars and 90% LTE representing transverse joint with dowel bars), and PCC slab temperature gradients (-4 °F/in, -2 °F/in, 0 °F/in, +2 °F/in, and +4 °F/in), all of which can significantly influence critical loading locations, were used.

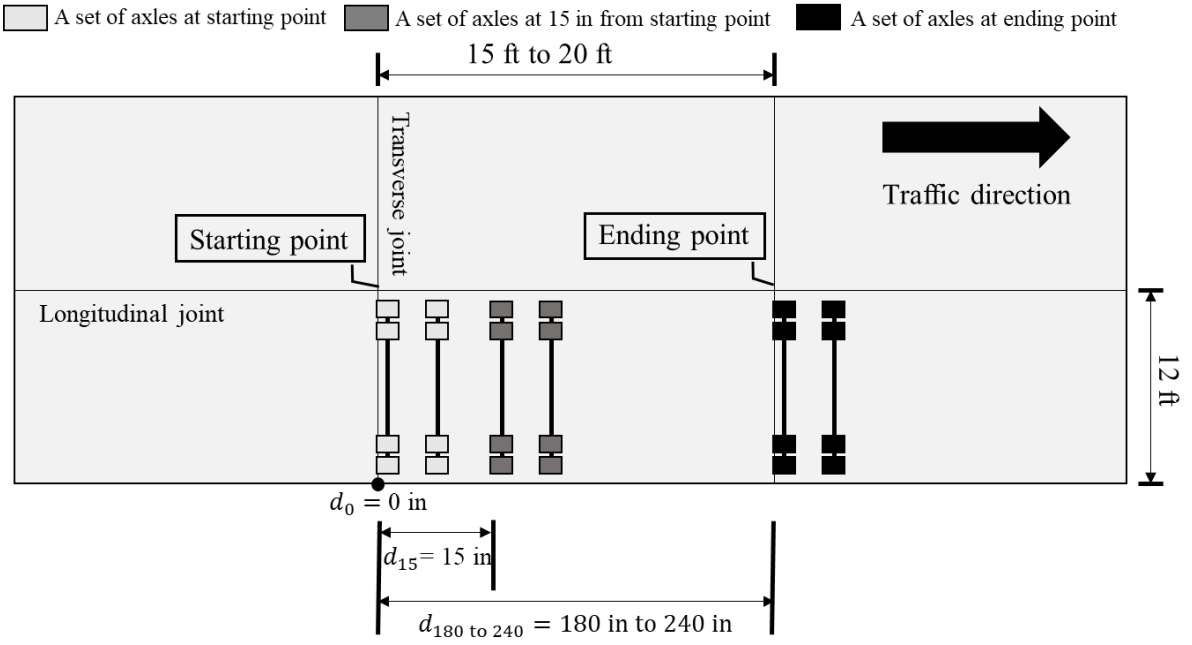

Figure 2. Loading locations across the PCC slab, note that d_{180} and d_{240} indicate a set of axles at ending points in slabs with 15 ft of transverse joint and 20 ft of transverse joint, respectively.

While the effect of loading locations on pavement responses using the influence-line approach has been investigated in previous studies (*13, 14*), only a few vehicles (e.g., FHWA classification vehicles or a few IoH types) have been investigated using influence-line analysis. Specifically, derivation of critical loading locations and classifications for various superload loading conditions have not been studied. In this study, by obtaining critical loading locations for superloads for as many as possible of the loading configurations used in recently released commercial superloads, they can be classified into several categories, so that the critical loading locations of the vehicles included in each category could then be easily derived.

Determination of Damage Ratio

Using the critical loading locations corresponding to each superload, the critical tensile stress at the bottom of the PCC layer and the critical tensile stress at the top of the PCC layer, the number of load repetitions to failure N_f can be obtained from analysis matrices that vary with respect to the JPCP properties. In more detail, the set of experimental matrices for FE analysis shown in **Table 3** can be established, with base inputs that include types of roads (i.e., local road and highway) and seasons (i.e., spring, summer, fall, and winter) directly related to the thickness of PCC layer and the composite modulus of subgrade reaction, respectively. The other subordinate inputs are the joint spacing, LTE, CTE, and temperature gradients of a PCC slab determined to correspond to a reasonable range of values representative of JPCP structures in Iowa. A total of 35 types of traffic loading, including 18 IoH types, 16 SHL types, and an FHWA class 9 truck (reference vehicle), were then considered as types of loading input for the FEA models. Altogether, considering payload levels of 100%, 75%, 50%, and 0% that each of the 34 superloads other than the reference vehicle can carry, a total of $34 \times 4 + 1 = 137$ traffic loadings were ultimately applied to each analysis model.

Table 3. Experimental matrices for the FE analysis

Local road					**Highway**			
Thickness of PCC layer (in)					**Thickness of PCC layer (in)**			
7, 9					10, 13			
Composite modulus of subgrade reaction (psi/in)					**Composite modulus of subgrade reaction (psi/in)**			
Season	**Spring**	**Summer**	**Fall**	**Winter**	**Spring**	**Summer**	**Fall**	**Winter**
	50	120	120	250	50	120	120	250
Transverse joint spacing (ft): 15					**Transverse joint spacing (ft):** 17, 20			
CTE (10^{-6}/°F): 4.3, 5.2					**CTE (10^{-6}/°F):** 4.3, 5.2			
Temperature gradients (°F /in): -4, -2, 0, 2, 4					**Temperature gradients (°F /in):** -4, -2, 0, 2, 4			
Elastic modulus of PCC layer (psi): 4×10^6					**Elastic modulus of PCC layer (psi):** 4×10^6			
Traffic loadings					**Traffic loadings**			
IoH: 18 types × 4 payload levels = 72 types SHL: 16 types × 4 payload levels = 64 types FHWA class 9 truck (reference): 1 type					IoH: 18 types × 4 payload levels = 72 types SHL: 16 types × 4 payload levels = 64 types FHWA class 9 truck (reference): 1 type			
Total analysis cases: 10,960 cases					**Total analysis cases: 21,920 cases**			

To quantify potential fatigue damages of JPCP structures under each type of superload, the damage ratio (D_r) concept, defined as the ratio of damage caused by superload loading to damage caused by the FHWA class 9 truck loading, was adopted. In this study, the damage ratios for two types of fatigue-related transverse cracking of PCC slab, including bottom-up transverse cracking and top-down transverse cracking, were obtained using **Equation 1** and **Equation 2**.

$$Damage\ ratio\ for\ bottom-up\ transverse\ cracking\ (D_b) = \frac{\frac{1}{N_{b,superload}}}{\frac{1}{N_{b,class\ 9}}} = \frac{N_{b,class\ 9}}{N_{b,superload}} \quad (1)$$

$$Damage\ ratio\ for\ top-down\ transverse\ cracking\ (D_t) = \frac{\frac{1}{N_{t,superload}}}{\frac{1}{N_{t,class\ 9}}} = \frac{N_{t,class\ 9}}{N_{t,superload}} \quad (2)$$

where, $N_{b,superload}$ = Number of load repetitions to failure due to tensile stress at the bottom of the PCC layer under superload;
$N_{b,class\ 9}$ = Number of load repetitions to failure due to tensile stress at the bottom of the PCC layer under FHWA class 9 truck;
$N_{t,superload}$ = Number of load repetitions to failure due to tensile stress at the top of the PCC layer under superload;
$N_{t,class\ 9}$ = Number of load repetitions to failure due to tensile stress at the top of the PCC layer under FHWA class 9 truck.

Obtaining the number of load repetitions to failure associated with both bottom-up transverse cracking and top-down transverse cracking required a transfer function appropriately reflecting the properties of the Iowa PCC slab, so an S-N curve using the ISU experimental results based on fatigue tests for the air-entrained concrete was drawn (*11, 12*). The material properties of the concrete beam used in this fatigue test were the same as those currently used for Iowa PCC slab construction. For example, an Iowa DOT C-3 mix having the properties of normal paving mix utilized in primary paving, Type 1 Portland cement with a 0.43 water-cement ratio, was used. Crushed limestone (specific gravity: 2.53, water absorption: 2.54%) from the Alden Quarry near Alden, Iowa, was applied as a coarse aggregate, while Hallett sand (specific gravity: 2.64, water absorption: 1.50%) was used as a fine aggregate. While ISU research workers had also applied air content over various ranges to confirm its effect on concrete fatigue strength, in this study, data from the 6.7% case, the closest to the most common air content used in the Iowa PCC slab, was used to draw the S-N curve shown in **Figure 3**. Note that the stress ratio, SR, is the ratio of flexural stress to the modulus of rupture.

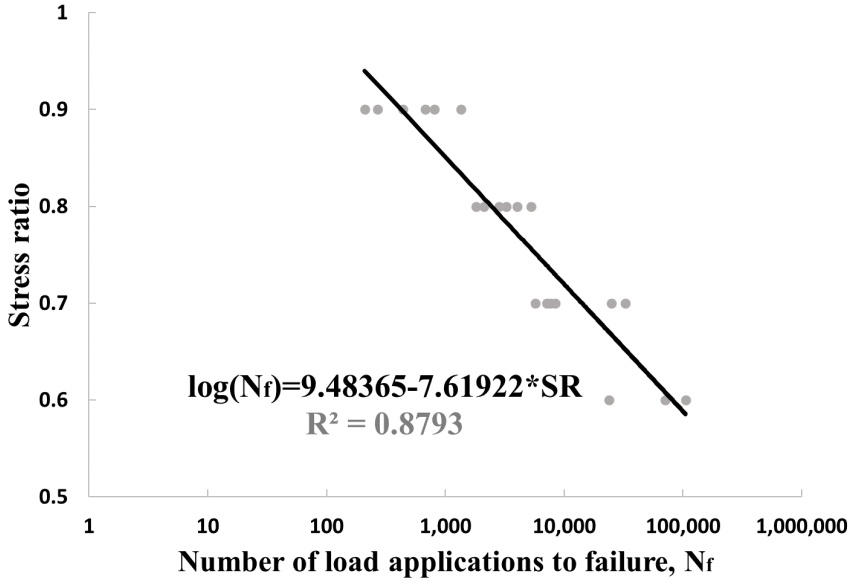

Figure 3. S-N curve created using data from previous experimental tests by ISU for PCC (*11, 12*).

For comparison, damage ratios using other transfer functions adopted from the Guide for Mechanistic-Empirical Design (*15*) and Portland Cement Association (*16*) were calculated in addition to those using transfer functions from previous ISU fatigue tests. **Equation 3** and **Equation 4** respectively show the transfer functions used to calculate the number of load repetitions to failure adopted from the Guide for Mechanistic-Empirical Design (*15*) and the Portland Cement Association (*16*). Note that the modulus of rupture of the PCC slab MR was calculated to be 662.5 psi, a value similar to the average modulus of rupture value of 667.2 psi calculated from six Iowa sections using long-term pavement performance (LTPP) data.

$$\log\left(N_{i,j,k,l,m,n}\right) = C_1 \cdot \left(\frac{MR_i}{\sigma_{i,j,k,l,m,n}}\right)^{C_2} + 0.4371 \tag{3}$$

$$\log N_f = 11.737 - 12.077\left(\frac{\sigma}{MR}\right) \qquad for\ \frac{\sigma}{MR} \geq 0.55 \tag{4-1}$$

$$\log N_f = \left(\frac{4.2577}{\frac{\sigma}{MR} - 0.4325}\right)^{3.268} \qquad for\ 0.45 < \frac{\sigma}{MR} < 0.55 \tag{4-2}$$

$$\log N_f = \text{unlimited} \qquad for\ \frac{\sigma}{MR} \leq 0.45 \tag{4-3}$$

where, $N_{i,j,k,l,m,n}$ = Allowable number of load applications at condition i, j, k, l, m, and n;
MR_i = PCC modulus of rupture at age i, psi; $MR = \frac{43.5E_c}{10^6} + 488.5$;
$\sigma_{i,j,k,l,m,n}$ = Applied stress at condition $i, j, k, l, m,$ and n;
C_1, C_2 = Calibration constant ($C_1 = 2.0, C_2 = 1.22$);
E_c = Modulus of elasticity of PCC slab.

CRITICAL LOADING LOCATIONS OF SUPERLOADS

In this section, critical loading locations are determined and categorized for each superload generating critical pavement responses, including tensile stress at the bottom of PCC slab and tensile stress at the top of PCC slab. By moving a set of axles representing loading configurations for each superload at 15-inch intervals from one transverse joint to the next transverse joint, it is possible to determine the level and location of critical pavement responses corresponding to each loading location. Since critical loading locations generating critical pavement responses vary mainly with respect to loading configuration and pavement properties, each critical loading location was determined by applying the different superload loading configurations to the FEA models and varying pavement properties (i.e., transverse joints [15 ft, 17 ft, and 20 ft], transverse joint LTE [50% LTE representing transverse joint without dowel bars and 90% LTE representing transverse joint with dowel bars], and temperature gradients of a PCC slab [-4 °F/in, -2 °F/in, 0 °F/in, +2 °F/in, and +4 °F/in]). Note that LTEs of both 50% and 90% were applied only to the JPCP model with 15 ft of transverse joint, while other models with 17 ft or 20 ft of transverse joint had only an LTE of 90% applied, reflecting realistic JPCP design practices in Iowa. **Figure 4** shows examples of critical loading locations for IoH and SHL on the JPCP with 15 ft for the transverse joint, 7 in for the PCC layer thickness, 50% for the LTE, and 0 °F/in for the temperature gradient. Because of the wide vehicle width in the IoH case, the tire-loading area often crosses a traffic lane, and due to their large vehicle size SHLs also usually operate on both traffic lanes, as can be seen in **Figure 4**.

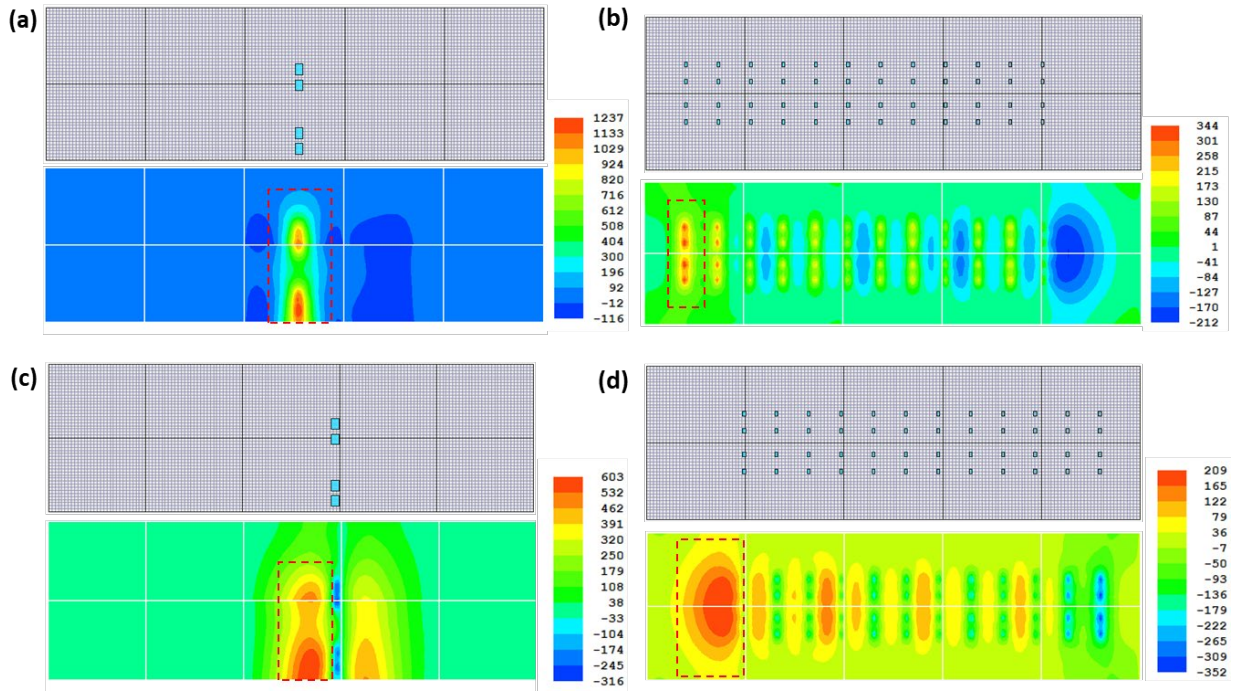

Figure 4. Critical loading locations on the JPCP with 15 ft for transverse joint, 7 in for thickness of PCC layer, 50% for LTE, and 0 °F/in for temperature gradient generating critical tensile stress: (a) at the bottom of PCC slab led by Kinze 1305 row crop, (b) at the bottom of PCC slab led by Goldhofer THP/SL-S, (c) at the top of PCC slab led by Kinze 1305 row crop, and (d) at the top of PCC slab led by Goldhofer THP/SL-S.

The resulting critical loading locations of IoHs and SHLs corresponding to the different pavement properties are categorized in **Table 4** and **Table 5**, respectively. Using categories associated with critical loading locations makes it easy to infer the critical loading location when a specific loading configuration is applied to a JPCP structure. The FEA results in this section indicate that temperature gradients do not affect the superload critical loading locations much differently than the individual loading level, so the effects of temperature gradients are not reflected in **Table 4** and **Table 5**.

Table 4. Categorization of critical loading locations following the loading configurations of IoHs

Case	Category	Type	Critical loading location	Relevant IoHs
Critical tensile stresses at the bottom of PCC slab	1	IoH with single-axle	Single-axle located near the mid-slab	Kinze 1305 flotation, Kinze 1305 row crop, Kinze 1051, J&M 1151
	2	IoH with tandem-axle	(2-1) For small axle spacing (< 86 in): tandem-axle located symmetrically within a PCC slab; (2-2) For high axle spacing (> 130 in): one of all axles locates near the mid-slab	(2-1) Balzer 1725, Balzer 6800 magnum, GEA EL48-4D (2-2) J&M 555 wagon, J&M 755 wagon
	3	IoH with tridem-axle	**[In case of JPCP with transverse joint: 15 ft, LTE: 50%]** (3-1) For small axle spacing (< 75 in): two of all axles located symmetrically within a PCC slab;	(3-1) GEA EL48-6D (3-2) Balzer 2550, Balzer 9500 magnum

			(3-2) For high axle spacing (> 78 in): one outer axle located on another slab away from the joint **[In case of JPCP with transverse joint: 15 ft and 17 ft, LTE: 90%]** (3-3) Two of all axles located symmetrically within a PCC slab **[In case of JPCP with transverse joint: 20 ft, LTE: 90%]** (3-4) All three axles are located symmetrically within a PCC slab	(3-3) and (3-4) GEA EL48-6D, Balzer 2550, Balzer 9500 magnum
	4	IoH with quad-axle	**[In case of JPCP with transverse joint: 15 ft and 17 ft, LTE: 50% and 90%]** (4-1) Two of all axles located symmetrically within a PCC slab **[In case of JPCP with transverse joint: 20 ft, LTE: 90%]** (4-2) Three of all axles located symmetrically within a PCC slab	(4-1) and (4-2) GEA EL48-8D, NUHN QT Quad Tanks
	5	IoH with a special type of axle configuration	Front axle located near the mid-slab	Terragator 2550, Terragator TG7300C, Terragator TG8400C, Case 340B
Critical tensile stresses at the top of PCC slab	1	IoH with single, tandem, tridem, or quad-axle	One outer axle located upon or near the transverse joint	Kinze 1305 flotation, Kinze 1305 row crop, Kinze 1051, J&M 1151, Balzer 1725, Balzer 6800 magnum, GEA EL48-4D, J&M 555 wagon, J&M 755 wagon, GEA EL48-6D, Balzer 2550, Balzer 9500 magnum, GEA EL48-8D, NUHN QT Quad Tanks
	2	IoH with a special type of axle configuration	One axle with the highest axle weight located upon or near the transverse joint	Terragator 2550, TerragatorTG 7300, Terragator TG8400C, Case 340B

Table 5. Categorization of critical loading locations following the loading configurations of SHLs

Case	Category	Type	Critical loading location	Relevant SHLs
Critical tensile stresses at the bottom of PCC slab	1	SHL with modular type trailers	**[In case of JPCP with transverse joint: 15 ft, LTE: 50% and 90%]** (1-1) The front or rear axle is located near the mid-slab, and only two axles, including the front or rear axle with the next axle, exist in a slab **[In case of JPCP with transverse joint: 17 ft, LTE: 90%]** (1-2) The first or last three axles are symmetrically located within a slab **[In case of JPCP with transverse joint: 20 ft, LTE: 90%]**	(1-1), (1-2), and (1-3) All the modular types of SHL

			(1-3) The first or last four axles are symmetrically located within a slab	
	2	SHL with drop-deck type trailers	Drop-deck type trailer with tandem-axle groups or tridem-axle groups located with the highest axle weight group in the same way as IoHs with a tandem-axle (2-1) or a tridem-axle (3-1) having small axle spacing from **Table 4**	All the drop-deck types of SHL
Critical tensile stresses at the top of PCC slab	1	SHL with modular type trailers	One outer axle located upon or near the transverse joint	All the modular types of SHL
	2	SHL with drop-deck type trailers	Drop-deck type trailer with tandem and tridem-axle groups located as two separate axle groups near transverse joints having one non-loaded PCC slab between them	All the drop-deck types of SHL

Examples of influence-line stress responses corresponding to distances of a set of axles from the starting point are presented in **Figure 5**. It should be noted that, for clarity, **Figure 5** includes only representative superloads from each category; the other superloads belonging to each category have critical loading locations similar to those of the representative superloads. In addition, as shown in **Figure 2**, a zero offset from the start point is defined when the last axle of all axles of each superload is positioned at the starting point. The graphs in **Figure 5** along with **Table 4** show that the critical loading locations of IoHs can be differentiated according to their numbers of axles and axle spacings. On the other hand, the modular types of SHL with relatively small and consistent axle spacings in **Figure 5** and **Table 5** generate critical tensile stresses primarily through front or rear axle loading, meaning that front or rear axle location would be the most critical factor in determining critical loading location. Unlike the modular type, drop-deck type SHLs have a relatively wide spacing between each group of axles, so that drop-deck type SHLs with tandem-axle groups (or tridem-axle groups) are subjected to the critical tensile stress at the bottom of PCC slab when the highest loaded axle group is located similarly to tandem-axle (or tridem-axle) IoHs. In the same vein, drop-deck type SHLs generate critical tensile stress at the top of PCC slab between the two highest loaded axle groups. As shown in this section, superloads, with non-standardized loading configurations, can be categorized according to their critical loading locations that are highly related to the type and spacing of their axles.

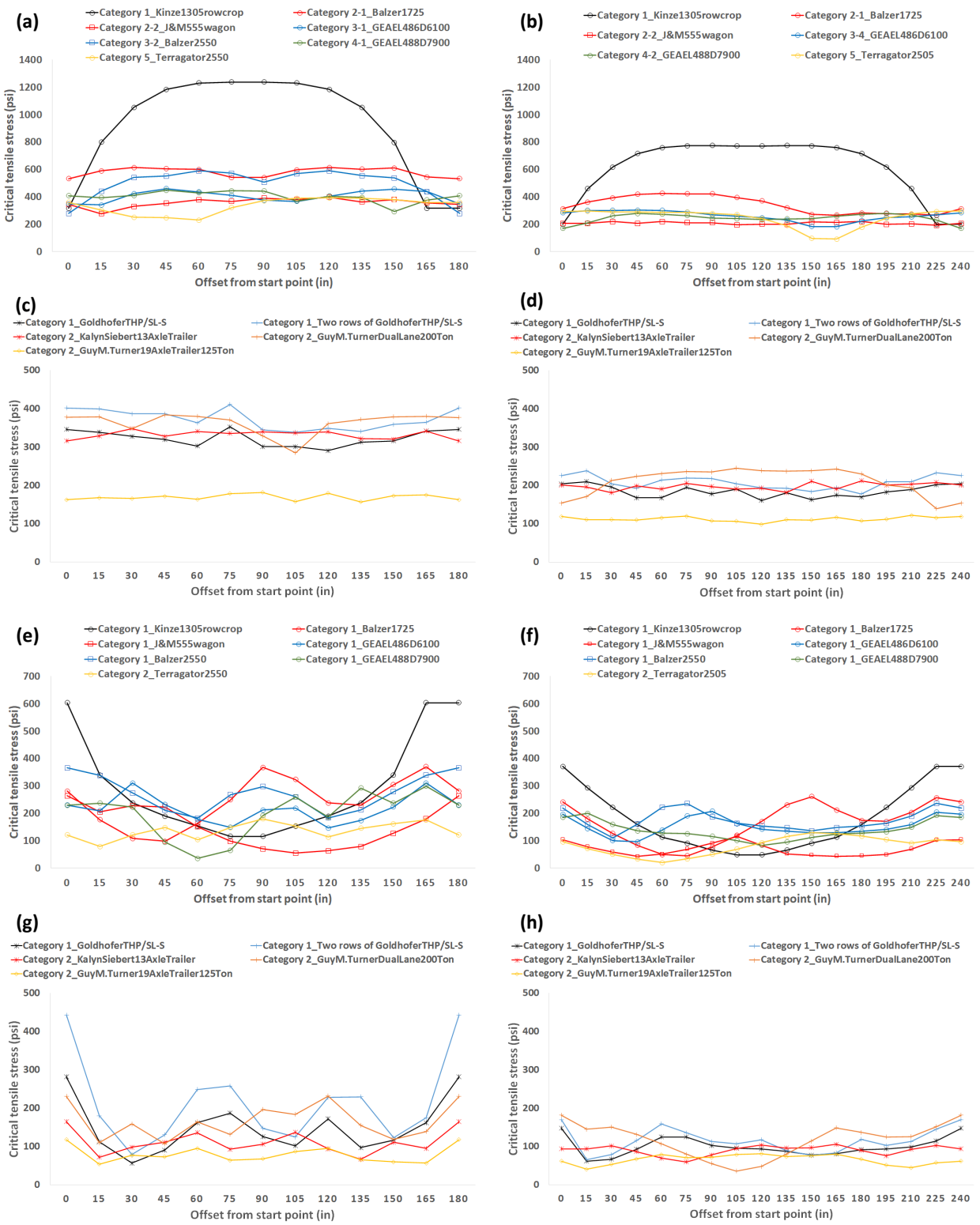

Figure 5. Examples of influence-line stress responses for critical tensile stress: (a) at the bottom of the PCC slab with 15 ft for transverse joint, 7 in for thickness of PCC layer, and 50% for transverse joint LTE under IoHs, (b) at the bottom of the PCC slab with 20 ft for transverse joint, 7 in for thickness of PCC layer, and 90% for transverse joint LTE under IoHs, (c) at the bottom of

the PCC slab with 15 ft for transverse joint, 7 in for thickness of PCC layer, and 50% for transverse joint LTE under SHLs, (d) at the bottom of the PCC slab with 20 ft for transverse joint, 7 in for thickness of PCC layer, and 90% for transverse joint LTE under SHLs, (e) at the top of the PCC slab with 15 ft for transverse joint, 7 in for thickness of PCC layer, and 50% for transverse joint LTE under IoHs, (f) at the top of the PCC slab with 20 ft for transverse joint, 7 in for thickness of PCC layer, and 90% for transverse joint LTE under IoHs, (g) at the top of the PCC slab with 15 ft for transverse joint, 7 in for thickness of PCC layer, and 50% for transverse joint LTE under SHLs, and (h) at the top of the PCC slab with 20 ft for transverse joint, 7 in for thickness of PCC layer, and 90% for transverse joint LTE under SHLS.

DAMAGE RATIO ANALYSIS

By considering the critical loading locations of each superload obtained in the previous section, a total of 32,880 FEA results related to bottom-up transverse cracking and top-down transverse cracking were obtained using the experimental matrices shown in **Table 3**. As mentioned earlier, a transfer function derived from previous ISU experimental data was used to convert critical pavement responses into values of the number of load repetitions to failure.

The degree of JPCP fatigue damage from experiencing superload traffic can be confirmed in terms of the number of load repetitions to failure through comparison with a FHWA class 9 truck (i.e., reference vehicle). Since the experimental matrices for FEA in **Table 3** reflect the full range of properties of Iowa JPCP, it is possible to check the degree of fatigue-related transverse crackings according to each type of IoH and type of SHL traveling on JPCP models, as shown in **Figure 6**. In addition, because the types and capacities of payloads carried by each type of superload are diverse, analysis of various payload levels ranging from 100% payload level (i.e., full loads) to 0% payload level (i.e., empty loads) should be performed to check relative fatigue damage dependent on the change of payload level.

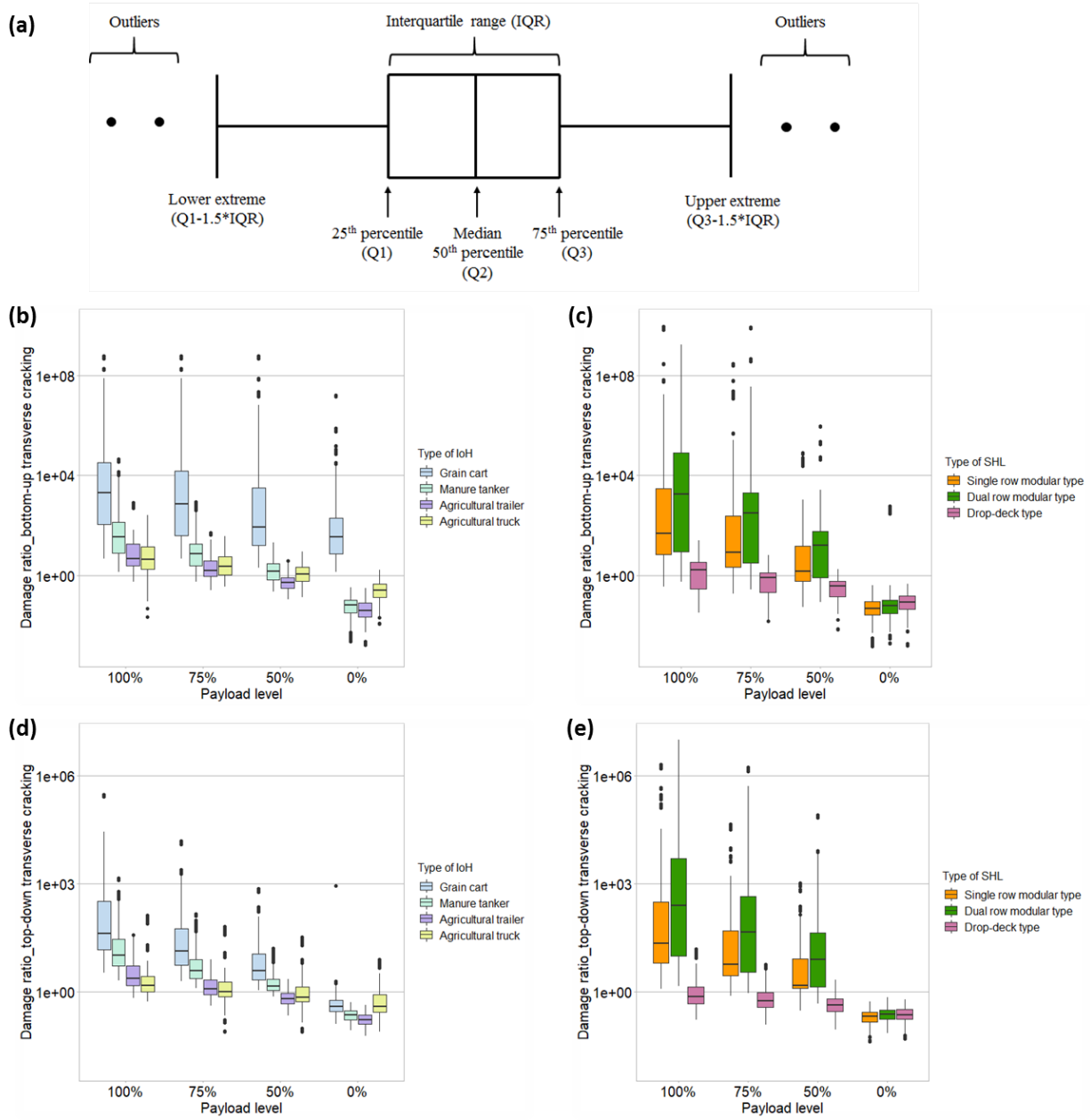

Figure 6. Damage ratio analysis results: (a) the configuration of box-whisker plot, (b) box-whisker plots comparing damage ratios based on bottom-up transverse cracking of PCC slabs under IoHs, (c) box-whisker plots comparing damage ratios based on bottom-up transverse cracking of PCC slabs under SHLs, (d) box-whisker plots comparing damage ratios based on the top-down transverse cracking of PCC slabs under IoHs, (e) box-whisker plots comparing damage ratios based on top-down transverse cracking of PCC slabs under SHLs.

As seen from the above box-whisker plots for IoH, grain-cart types tend to generate more significant fatigue-related transverse cracking than other types of IoH. Grain carts and manure tankers at all payload levels except for the 0% payload also exhibit damage ratios greater than one for both bottom-up transverse cracking and top-down transverse cracking, while agricultural trailers and agricultural trucks show relatively lower damage ratios, and when carrying 50% payload or lower, even less than one

in some JPCP models. Overall, most IoHs except for grain carts cause fatigue damage similar to FHWA class 9 trucks when carrying a 50% payload.

In the case of SHLs, most FEA results except for the empty-load case show that modular type SHLs cause significantly greater fatigue-related transverse cracking compared to drop-deck type SHLs. These results clearly show that, despite drop-deck type SHLs being heavier than modular type SHLs, modular types with much higher load capacity cause severe fatigue-related transverse cracking at payload levels equal to or greater than 50%. As a result, drop-deck type SHLs cause similar or even less fatigue damage than FHWA class 9 trucks for all payload levels, while modular type SHLs are likely to cause significant fatigue damages at payload levels of 50% or more.

To compare damage ratios produced by transfer function calculation from previous ISU fatigue tests, other transfer functions adopted from the Guide for Mechanistic-Empirical Design (*15*) and the Portland Cement Association (*16*) were used to calculate damage ratios under the same analysis conditions. **Table 6** and **Table 7** show that damage ratios calculated from the transfer functions of the Guide for Mechanistic-Empirical Design and the Portland Cement Association exhibit an exaggeratedly-wider range than damage ratios calculated using the transfer function derived from the ISU fatigue tests. However, damage ratios from superloads for both bottom-up transverse cracking and top-down transverse cracking exhibit similar trends corresponding to each payload level for all three transfer functions. Please note that the damage ratios shown in **Table 6** and **Table 7** are the overall damage ratios for all IoH or SHL types, while **Figure 6** shows the damage ratios for each type of IoH or SHL.

Table 6. Damage ratios of IoHs using different transfer functions

Transfer function		**100% payload**	**75% payload**	**50% payload**	**0% payload**
		Damage ratio of IoH (bottom-up transverse cracking)			
Guide for Mechanistic-Empirical Design (*15*)	Max.	1.24E+37 (Grain cart)	3.29E+35 (Grain cart)	4.24E+32 (Grain cart)	2.86E+6 (Grain cart)
	Median	7.69E+5	5.41E+10	1.71E+4	3.26E-24
	Min.	9.85E+9 (Agricultural truck)	1.17E-21 (Agricultural truck)	7.79E-47 (Agricultural truck)	< 1.00E-100 (Agricultural trailer)
ISU fatigue tests (*11, 12*)	Max.	7.38E+10 (Grain cart)	1.53E+8 (Grain cart)	3.17E+5 (Grain cart)	2.12E+0 (Grain cart)
	Median	3.28E+1	1.42E+1	1.86E+0	1.14E-1
	Min.	2.57E-1 (Agricultural truck)	1.08E-1 (Agricultural truck)	2.16E-2 (Agricultural trailer)	1.57E-3 (Agricultural trailer)
Portland Cement Association (*16*)	Max.	2.33E+17 (Grain cart)	1.20E+13 (Grain cart)	6.16E+8 (Grain cart)	3.32E+0 (Grain cart)
	Median	2.64E+2	2.51E+1	2.70E+0	3.12E-2
	Min.	1.14E-1 (Agricultural truck)	2.86E-2 (Agricultural trailer)	2.18E-3 (Agricultural trailer)	3.29E-5 (Agricultural trailer)
Transfer function		**Damage ratio of IoH (top-down transverse cracking)**			
Guide for Mechanistic-Empirical Design (*15*)	Max.	1.04E+48 (Grain cart)	5.95E+44 (Grain cart)	1.03E+39 (Grain cart)	7.25E+13 (Agricultural truck)
	Median	6.64E+12	1.15E+10	1.57E+5	1.75E-42
	Min.	5.92E-22	< 1.00E-100	< 1.00E-100	< 1.00E-100

		(Agricultural truck)	(Agricultural truck)	(Agricultural truck)	(Agricultural trailer)
ISU fatigue tests (*11, 12*)	Max.	3.00E+5 (Grain cart)	1.51E+4 (Grain cart)	7.44E+2 (Grain cart)	8.10E+0 (Agricultural truck)
	Median	8.95E+0	5.21E+0	1.62E+0	2.97E-1
	Min.	5.43E-1 (Agricultural truck)	4.20E-1 (Agricultural truck)	8.11E-2 (Agricultural trailer)	6.04E-2 (Agricultural trailer)
Portland Cement Association (*16*)	Max.	5.66E+8 (Grain cart)	4.77E+6 (Grain cart)	3.88E+4 (Grain cart)	2.83E+1 (Agricultural truck)
	Median	8.48E+1	3.32E+1	2.15E+1	1.44E-1
	Min.	3.76E-1 (Agricultural truck)	1.81E-2 (Agricultural truck)	1.69E-2 (Agricultural truck)	1.13E-2 (Agricultural trailer)

Table 7. Damage ratios of SHLs using different transfer functions

Transfer function		**100% payload**	**75% payload**	**50% payload**	**0% payload**
		Damage ratio of SHL (bottom-up transverse cracking)			
Guide for Mechanistic-Empirical Design (*15*)	Max.	6.34E+37 (Dual row modular type)	1.25E+36 (Dual row modular type)	2.51E+32 (Dual row modular type)	2.56E-5 (Dual row modular type)
	Median	6.94E+5	1.14E+4	1.86E+1	8.10E-48
	Min.	3.56E-56 (Drop-deck type)	2.62E-81 (Drop-deck type)	< 1.00E-100 (Drop-deck type)	< 1.00E-100 (Single row modular type)
ISU fatigue tests (*11, 12*)	Max.	7.16E+13 (Dual row modular type)	8.15E+9 (Dual row modular type)	9.30E+5 (Dual row modular type)	5.79E+2 (Dual row modular type)
	Median	2.48E+1	1.11E+1	5.41E+0	5.79E-2
	Min.	3.09E-2 (Drop-deck type)	1.46E-2 (Drop-deck type)	6.86E-3 (Drop-deck type)	1.43E-3 (Single row modular type)
Portland Cement Association (*16*)	Max.	1.38E+22 (Dual row modular type)	6.89E+15 (Dual row modular type)	3.45E+9 (Dual row modular type)	2.60E+4 (Dual row modular type)
	Median	1.69E+2	1.49E+1	1.18E+0	1.05E-2
	Min.	3.87E-3 (Drop-deck type)	1.16E-3 (Drop-deck type)	3.49E-4 (Drop-deck type)	2.86E-5 (Single row modular type)
Transfer function		**Damage ratio of SHL (top-down transverse cracking)**			
Guide for Mechanistic-Empirical Design (*15*)	Max.	5.19E+52 (Dual row modular type)	3.30E+50 (Dual row modular type)	9.58E+45 (Dual row modular type)	1.96E-4 (Dual row modular type)
	Median	1.45E+14	3.97E+11	6.96E+4	1.53E-75
	Min.	< 1.00E-100 (Drop-deck type)	< 1.00E-100 (Drop-deck type)	< 1.00E-100 (Drop-deck type)	< 1.00E-100 (Single row modular type)

ISU fatigue tests (*11, 12*)	Max.	1.51E+7 (Dual row modular type)	9.76E+6 (Dual row modular type)	8.00E+4 (Dual row modular type)	7.28E-1 (Dual row modular type)
	Median	1.37E+1	4.48E+0	1.47E+0	2.27E-1
	Min.	1.68E-1 (Drop-deck type)	1.25E-1 (Drop-deck type)	9.28E-2 (Drop-deck type)	4.30E-2 (Single row modular type)
Portland Cement Association (*16*)	Max.	2.98E+11 (Dual row modular type)	1.47E+11 (Dual row modular type)	6.85E+7 (Dual row modular type)	6.03E-1 (Dual row modular type)
	Median	6.55E+1	1.10E+1	1.85E+0	9.35E-2
	Min.	5.77E-2 (Drop-deck type)	3.59E-2 (Drop-deck type)	2.24E-2 (Drop-deck type)	6.56E-3 (Single row modular type)

EVALUATION OF STRUCTURAL BENEFITS OF SHOULDER TYPES ON JPCP UNDER SUPERLOADS

The FEA performed in the previous sections used models without considering any shoulders, assumed to be granular. The reason for not including such shoulders (i.e., granular shoulder application) in the FEA models is that most county roads in Iowa, the target state of this study, have granular rather than paved shoulders (*17*). However, it is still necessary to check the performance of JPCPs according to different shoulder alternatives, including tied PCC or HMA shoulders. In this section, we re-determined the critical loading location of each superload from FEA matrices that simulated different shoulder alternatives and compared the critical pavement responses to those applying the critical loading location as a loading condition. To this end, the following shoulder alternatives were added and applied to the existing FEA models shown in **Table 3**. Please note that the thicknesses of the PCC layer and transverse joint spacing were fixed at 10 in and 20 ft, respectively, from the experimental matrices in **Table 3** due to the excessive number of analysis cases resulting from the inclusion of three different shoulder types when determining critical pavement responses.

- Granular shoulder: no shoulder applied;
- Full-depth tied PCC shoulder: the shoulder thickness is the same as the PCC slab (10 in); the shoulder width is 8 ft for both lanes; the LTE between the PCC slab and the shoulder is applied at 50% and 70%, referring to the Guide for Mechanistic-Empirical Design (*18*);
- Partial-depth HMA shoulder: the shoulder thickness is less than that of the PCC slab (8 in); the shoulder width is 8 ft for both lanes; the LTE between the PCC slab and the shoulder is applied at 10%, referring to the Guide for Mechanistic-Empirical Design (*18*).

Prior to comparing the critical pavement responses of JPCPs according to each shoulder alternatives application, the critical loading location for each superload in JPCP structure to which each type of shoulder was applied was obtained, again using the influence line-analysis approach (*10*), as shown in **Figure 7**. The critical loading locations were re-determined by applying the various pavement properties (i.e., transverse joints [15 ft, 17 ft, and 20 ft], transverse joint LTE [50% and 90%], and temperature gradients of a PCC slab [-4 °F/in, -2 °F/in, 0 °F/in, +2 °F/in, and +4 °F/in]) to check whether the categorization of critical loading locations following the loading configurations of IoHs and SHLs shown in **Table 4** and **Table 5** is still valid for the different shoulder alternatives. A randomly-selected superload for each category was intensively analyzed to determine critical loading locations and corresponding critical pavement responses in terms of both bottom-up PCC slab transverse cracking and top-down transverse cracking.

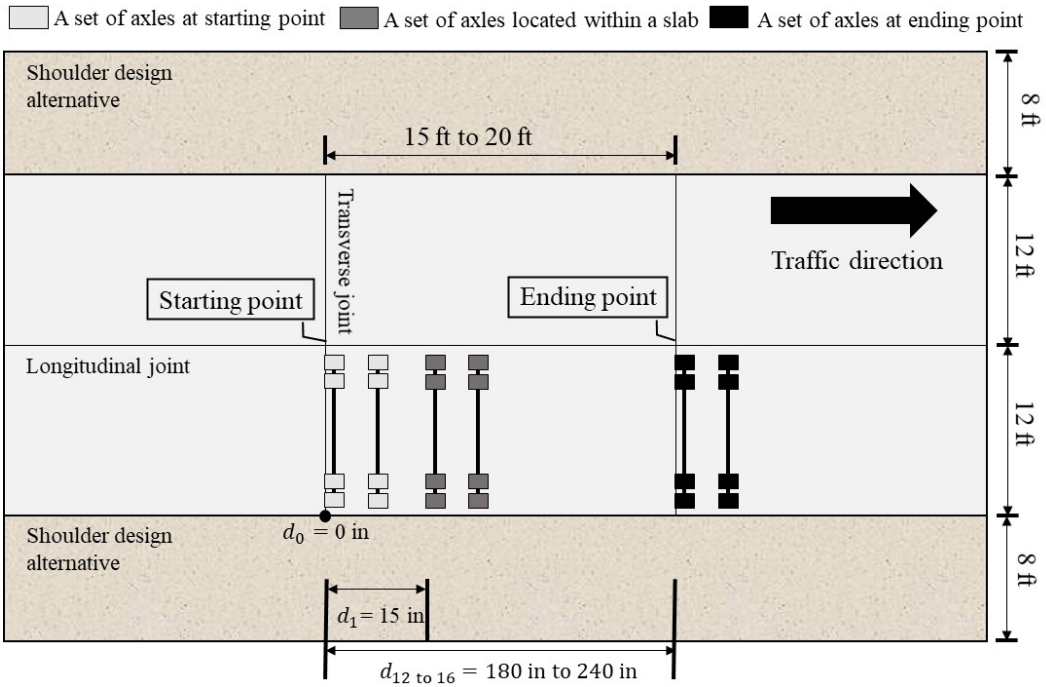

Figure 7. Loading locations across the PCC slab applying shoulder alternatives, note that d_{180} and d_{240} indicate a set of axles at ending points in slabs with 15 ft of transverse joint and 20 ft of transverse joint, respectively.

The FEA results for JPCPs with different shoulder alternatives confirmed that the critical loading locations of representative types of superload could be categorized in the same way as the granular shoulder for other shoulder alternatives, including full-depth PCC and partial-depth HMA shoulders. This means that a randomly-selected superload per category traveling on JPCPs with a full-depth tied PCC shoulder or a partial-depth HMA shoulder encounters critical loading locations similar to JPCPs with granular shoulders for both critical tensile stresses at the bottom of the PCC slab and the top of the PCC slab. The critical loading locations of an example IoH from Category 1 are shown in **Figure 8**.

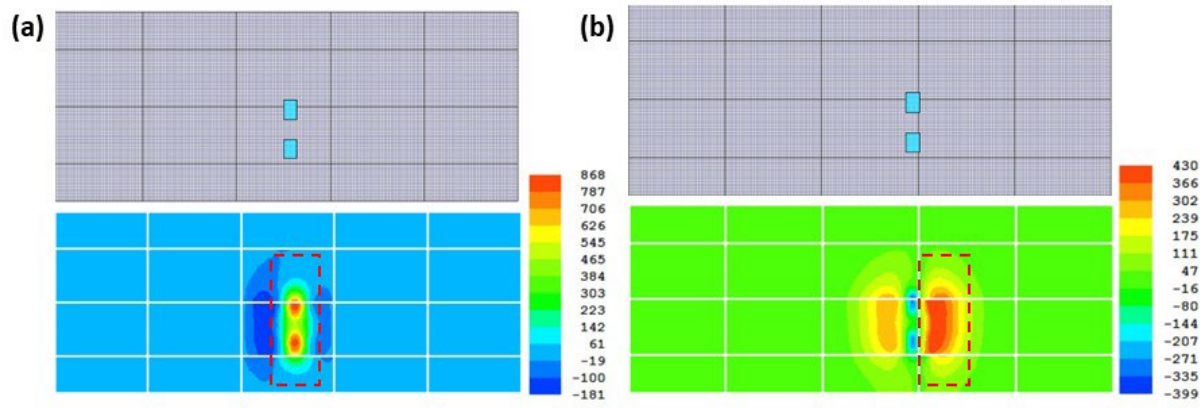

Figure 8. Critical loading locations generating critical tensile stress: (a) at the bottom of PCC slab and (b) at the top of PCC slab led by Kinze 1305 flotation from category 1 on the JPCPs having 20 ft of transverse joint spacing, 10 in of PCC thickness, -2°F/in of temperature gradient, and the full-depth tied PCC shoulder with 70% LTE between PCC slab and shoulder.

As a final step, the critical pavement responses at the bottom and top of the PCC slab were determined from FEA models representing different types of the shoulder by applying critical loading conditions of representative superloads of each category carrying 100% payload levels. **Figure 9** shows how much of the critical pavement response the representative superload of each category on each paved shoulder model produces, on average, compared to that produced by the granular shoulder models.

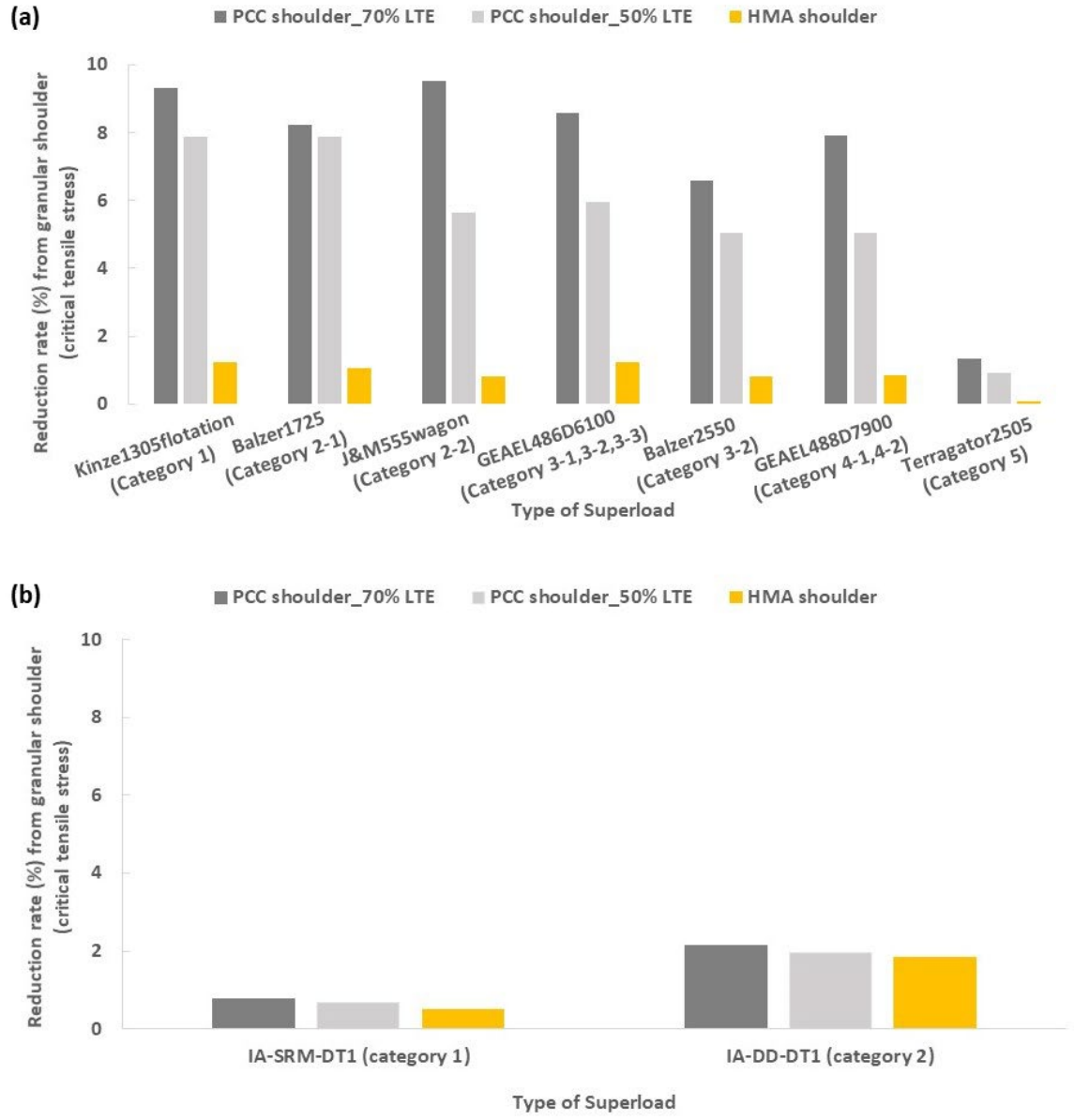

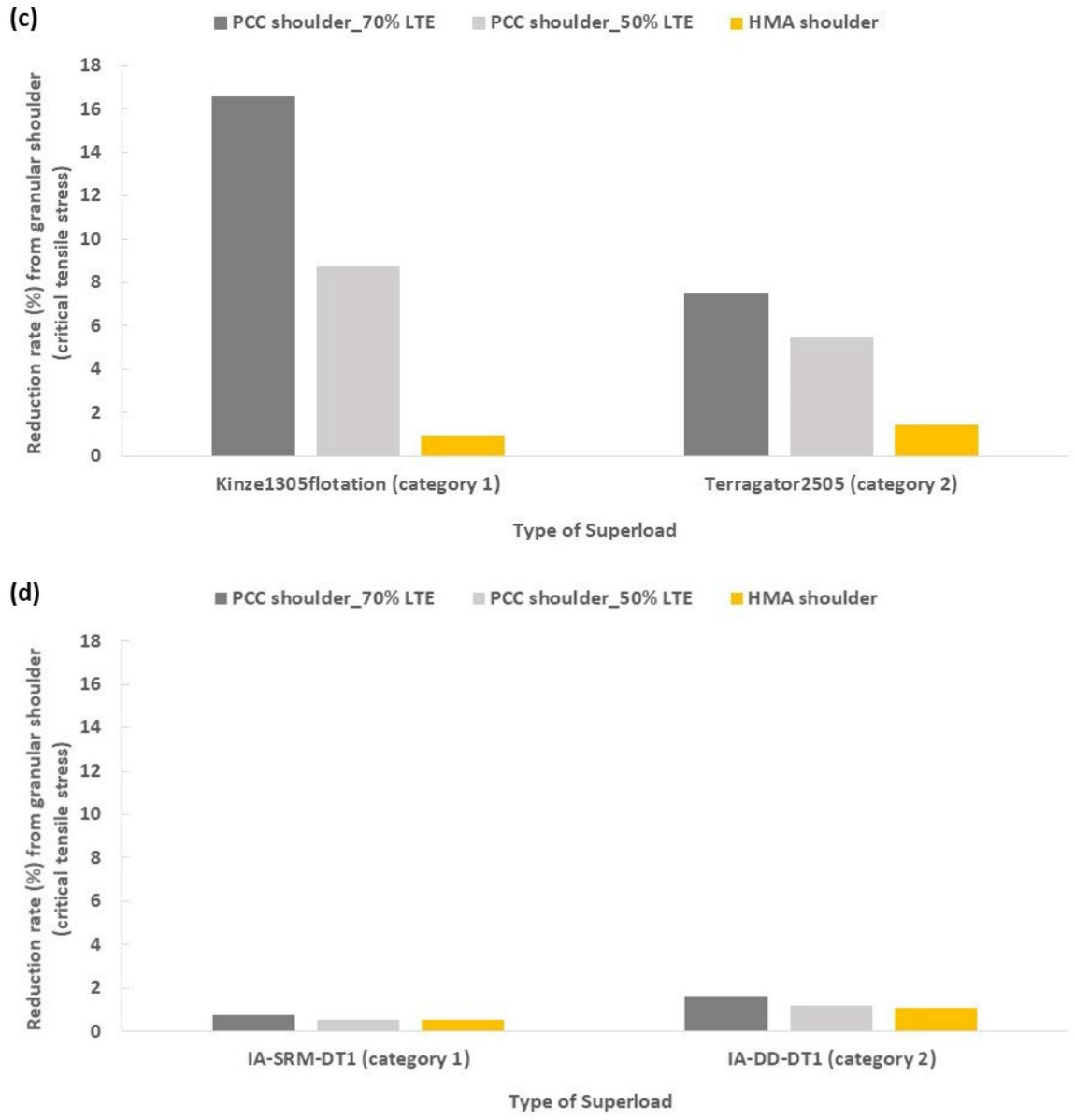

Figure 9. Reduction rate of critical tensile stress compared to the granular shoulder models: (a) at the bottom of PCC slab under IoHs, (b) at the bottom of PCC slab under SHLs, (c) at the top of PCC slab under IoHs, and (d) at the top of PCC slab under SHLs.

As can be seen from these results, the critical tensile stresses of JPCPs produced by IoHs were significantly reduced when full-depth PCC shoulders were present. For example, in the case of the FEA models with 70% LTE between PCC slab and PCC shoulder, critical tensile stresses at the bottom of the PCC slab were reduced by about 9.3% on average, while critical tensile stresses at the top of the PCC slab were reduced by about 16.6% on average when led by the Kinze1305flotation determination. On the other hand, SHLs exhibited a relatively small reduction in critical tensile stresses when paved shoulders were applied because SHLs operate on both lanes due to their large vehicle size. So, while the results were less affected by the additional paved shoulder application in this analysis, the use of paved shoulders can provide an additional option of operating SHLs in one lane when that lane is wide enough to carry large-sized vehicles.

CONCLUSIONS AND RECOMMENDATIONS

Finite Element Analysis (FEA) was conducted to determine the critical loading location of each superload-generated critical pavement response by adopting the influence-line analysis approach to predict fatigue-related transverse cracking damage to Jointed Plain Concrete Pavements (JPCP) under superloads (*10*). Critical pavement responses of JPCP under critical loading conditions by each superload were calculated by performing FEAs of more than 32,000 analysis cases, and then the results were converted to damage ratios using various available transfer functions derived from concrete fatigue-test results. The main conclusions of this study can be summarized as follows:

- Critical loading locations of Implements of Husbandry (IoH) with respect to the critical tensile stress at the bottom of Portland cement concrete (PCC) slabs are related to axle configuration and the transverse joint and Load Transfer Efficiency (LTE) of the PCC slab as follows: (i) single-axle located near the mid-slab for the single-axle trailer; (ii) tandem-axle located symmetrically within a PCC slab for a tandem-axle trailer with small axle spacing (< 86 in); (iii) one of all axles located near the mid-slab for the tandem-axle trailer with high axle spacing (> 130 in); (iv) two of all axles located symmetrically within a PCC slab for the tridem-axle trailer on JPCPs with 15 ft and 17 ft of transverse joint and 90% of LTE, and for a tridem-axle trailer with small axle spacing (< 75 in) on JPCPs with 15 ft of transverse joint and 50% of LTE; (v) one outer axle located on an adjacent slab away from the joint for a tridem-axle trailer with high axle spacing (> 78 in) on JPCPs with 15 ft of transverse joint and 50% of LTE; (vi) all three axles located symmetrically within a PCC slab for the tridem-axle trailer on JPCPs with 20 ft of transverse joint and 90% of LTE; (vii) two of all axles located symmetrically within a PCC slab for the quad-axle trailer on JPCPs with 15 ft and 17 ft of transverse joint and 50% and 90% of LTE; (viii) three of all axles located symmetrically within a PCC slab for the quad-axle trailer on JPCPs with 20 ft of transverse joint and 90% of LTE; (ix) front axle located near mid-slab for a special trailer type;
- Critical loading locations of IoHs with respect to the critical tensile stress at the top of the PCC slab depend primarily on axle configuration as follows: (i) one outer axle located upon or near the transverse joint for single, tandem, tridem and quad-axle trailer; (ii) one axle with the highest axle weight located upon or near the transverse joint for a special type of trailer;
- Critical loading locations of Superheavy Loads (SHL) with respect to the critical tensile stress at the bottom of PCC slab depend primarily on the trailer type and the transverse joints of the PCC slab as follows: (i) front or rear axles located near the mid-slab, and only two axles, including the front or rear axle along with the adjacent axle, existing in the same slab, for a modular type trailer on JPCPs with 15 ft of transverse joint and 50% and 90% of LTE; (ii) first or last three axles symmetrically located within a slab for a modular type trailer on JPCPs with 17 ft of transverse joint and 90% of LTE; (iii) first or last four axles symmetrically located within a slab for a modular type trailer on JPCPs with 20 ft of transverse joint and 90% of LTE; (iv) a drop-deck type trailer with tandem-axle groups or tridem-axle groups located with the highest axle weight group in the same way as IoHs with a tandem-axle or a tridem-axle having small axle spacing;
- Critical loading locations of SHLs with respect to the critical tensile stress at the top of the PCC slab depend primarily on trailer type as follows: (i) one outer axle located upon or near the transverse joint for a modular trailer type; (ii) a drop-deck type trailer with tandem and tridem-axle groups located as two separate axle groups near transverse joints having one non-loaded PCC slab between them;
- In the case of IoHs, most grain-cart types generate more significant bottom-up transverse cracking and top-down transverse cracking of PCC slab than other types of IoH. Moreover, grain carts and manure tankers at all payload levels except 0% exhibit fatigue damage ratios greater than one. At the same time, agricultural trailers and agricultural trucks exhibit relatively lower damage ratios, even lower than one for some JPCP models when carrying a 50% payload or

lower. Overall, most IoHs except for grain carts cause fatigue damage similar to that of Federal Highway Administration (FHWA) class 9 trucks when carrying a 50% payload level;

- In the case of SHLs, most FEA results except for the 0% payload case show that modular type SHLs cause significantly greater fatigue-related transverse cracking than drop-deck type SHLs. Drop-deck type SHLs cause similar or even lesser fatigue damages than FHWA class 9 trucks at all payload levels, while modular type SHLs are likely to cause significant fatigue damages more than those for FHWA class 9 trucks for payload levels of 50% or more;
- JPCP structures with different shoulder alternatives such as granular shoulder, full-depth PCC shoulder, and partial-depth HMA shoulder have similar critical loading locations for representative types of superload to those categories derived in the previous sections. This means that a randomly-selected superload per category traveling over JPCPs with full-depth tied PCC shoulder and partial-depth HMA shoulder exhibits similar critical loading locations to those for JPCPs with a granular shoulder with respect to both critical tensile stresses at the bottom of the PCC slab and the top of the PCC slab;
- Critical tensile stresses of JPCPs carrying IoHs are significantly reduced when full-depth PCC shoulders are used, while SHLs exhibit only a relatively small reduction of critical tensile stresses when paved shoulders are used. This is mainly related to the position of the axle loadings (i.e., offset from the edge of PCC slab or wandering of axle loadings).

ACKNOWLEDGEMENTS

The authors gratefully acknowledge the Iowa Highway Research Board and the Iowa Department of Transportation for supporting this study. The project technical advisory committee (TAC) members from Iowa county engineers, including Lee Bjerke, Zach Gunsolley, Todd Kinney, Brian Moore, Mark Nahra, John Riherd, Brad Skinner, Jacob Thorius, and Danny Waid, are gratefully acknowledged for their guidance, support, and direction throughout the research. The authors would also like to express their sincere gratitude to other research team members from Iowa State University's PROSPER at the InTrans for their assistance. The contents of this paper reflect the views of the authors who are responsible for the facts and accuracy of the data presented within. The contents do not necessarily reflect the official views and policies of the Iowa Highway Research Board, the Iowa Department of Transportation, or Iowa State University. This paper does not constitute a standard, specification, or regulation.

AUTHOR CONTRIBUTION STATEMENT

The authors confirm contribution to the paper as follows: study conception and design: Drs. Halil Ceylan, Sunghwan Kim, and In-Ho Cho; data collection: Yongsung Koh; analysis and interpretation of results: Yongsung Koh, Drs. Halil Ceylan, Sunghwan Kim, and In-Ho Cho; draft manuscript preparation: Yongsung Koh, Drs. Halil Ceylan, Sunghwan Kim, and In-Ho Cho. All authors reviewed the results and approved the final version of the manuscript.

DECLARATION OF CONFLICTING INTERESTS

The authors declare that they have no conflict of interests with respect to the research, authorship, and/or publication of this article.

FUNDING

The research is supported by the Iowa Highway Research Board and the Iowa Department of Transportation (Grants IHRB-187).

REFERENCES

1. Kim, D., R. Salgado, and A. G. Altschaeffl. Effects of supersingle tire loadings on pavements. *Journal of Transportation Engineering*, 2005, 131(10), pp.732-743.

2. Huhtala, M., J. Pihlajamaki, and M. Pienimaki. Effects of tires and tire pressures on road pavements. *Transportation research record*, 1989, 1227, pp.107-114.

3. Ceylan, H., S. Wang, S. Kim, K. Gopalakrishnan, L. Khazanovich, and S. Dai. Impact of farm equipment loading on low-volume concrete road structural response and performance. *The Baltic Journal of Road and Bridge Engineering*, 2015, 10(4), pp.325-332.

4. Lim, J., A. Azary, L. Khazanovich, S. Wang, S. Kim, H. Ceylan, and K. Gopalakrishnan. *Effects of Implements of Husbandry (Farm Equipment) on Pavement Performance*. MN/RC 2012-08, Minnesota Department of Transportation, 2012.

5. Phares, B. M., T. J. Wipf, and H. Ceylan. *Impacts of Overweight Implements of Husbandry on Minnesota Roads and Bridges*. MN/RC – 2005-05, Minnesota Department of Transportation, 2004.

6. Papagiannakis, A. T. *Practices for Permitting Superheavy Load Movements on Highway Pavements.* NCHRP Sybthesis 476, TRB, 2015.

7. Stone, J. R., M. Kowalsky, R. Hughes, C. K. Herrick, B. Narron, and W. Cao. *Analysis of Truck Load Weight Distribution in North Carolina*. North Carolina Department of Transportation, 2012.

8. *Motor Vehicles and Law of the Road*. Iowa Code §§ 321.463. 2021.

9. ERES Consultants. *ISLAB2000 Finite Element Code for Rigid Pavement Analysis*. Version 3.6, Champaign, Illinois, 1999.

10. Byrum, C. R., and W. Hansen. Influence function approach to analysis of jointed portland cement concrete pavement. *Transportation Research Record*, pp.148-148. 1994.

11. Klaiber, F. W., T. L. Thomas, and D. Y. Lee. *Fatigue Behavior of Air-entrained Concrete: Phase II*. No. HR-197, Iowa State University, 1979.

12. Coleman. J. W. *Fatigue Behavior of Air-entrained Concrete.* PhD diss., Iowa State University, 1977.

13. Hiller, J. E., and J. R. Roesler. Determination of critical concrete pavement fatigue damage locations using influence lines. *Journal of Transportation Engineering*, 2005, 131(8), pp.599-607.

14. Wang, S., H. Ceylan, H., S. Kim, K. Gopalakrishnan, L. Khazanovich, and S. Dai. *Impact of farm equipment loading on rigid pavement performance using finite element analysis*. In *10th International Conference on Concrete Pavement*, Quebec City, Quebec, Canada, 2012.

15. *Guide for Mechanistic–Empirical Design of New and Rehabilitated Pavement Structures*. NCHRP Project 1-37A, Final Report, Applied Research Associates, Inc., ERES Consultants Division, 2004.

16. Packard, R. G., and S. D. Tayabji. New PCA thickness design procedure for concrete highway and street pavements. In *Third International Conference on Concrete Pavement Design and Rehabilitation*, Purdue University, West Lafeyette, Indiana, 1985.

17. Souleyrette, R., T. McDonald, Z. Hans, A. Kamyab, T. Welch, and B. Storm. *Paved shoulders on primary highways in Iowa: An analysis of shoulder surfacing criteria, costs, and benefits.* No. Final Report, 2001.

18. NCHRP Project 1-37A. *Development of the 2002 Guide for the Design of New and Rehabilitated Pavement Structures: Phase II. Part III Design analysis.* Transportation Research Board of the National Academies, Washington, D.C., Feb. 2004.